





### 33 **1. Introduction**

34 During the transmission of GPS signals from satellite to receiver, the signals  
35 propagate through the ionosphere so that the ionospheric delay is closely associated  
36 with GPS and is considered one of the main sources of errors in point positioning  
37 using GPS techniques, on the other hand GPS can be used as a sensor of the  
38 ionosphere and investigate its characteristics because of the global system coverage  
39 and the availability of multiple frequency data.

40 In this paper we used GPS receiver as a sensor of the ionosphere. The ionosphere  
41 is a dispersive medium, which means that the delay depends on the frequency of  
42 the signal. the first order effect of the ionosphere refraction could be eliminated  
43 mathematically by means of a linear combination of the signals on the two  
44 frequencies, because GPS signals are broadcast on more than one frequency. This  
45 combination is widely called the iono-free combination (Leandro, 2009).

46 Various methods were devised to calculate the ionospheric delay. These methods  
47 were based on spherical harmonic expansions in the global or regional scale (e.g.  
48 Schaer, 1999, and Wielgosz et al., 2003a). Local methods were based on two-  
49 dimensional Taylor series expansions (e.g. Komjathy, 1997, Jakobsen et al. 2010,  
50 Deng et al 2009, and Masaharu et al. 2013).

51 This paper is aimed to apply Precise Point Positioning (PPP) observation for  
52 accurate ionosphere error modeling, using carrier phase measurements the  
53 proposed algorithm was written using MATLAB.

### 54 **2. Observations equations for carrier-phase measurements.**

55 The observations of dual-frequency GPS receiver at any station consists of two codes  
56 and two carrier phase observations in RINEX format which were used for present  
57 model. The observations equations for carrier-phase measurements can be  
58 formulated as follows (Leandro, 2009; e.g. Sedeek et al., 2017):

$$59 \quad \Phi = R + c(dT - dt) + T - I + \lambda N + pbr - pbs + hdr - hds + m + e \quad (1)$$

60 Where  $\Phi$ ,  $R$ ,  $C$ ,  $dT$  and  $dt$ ,  $T$ ,  $I$ ,  $\gamma$ ,  $N$ ,  $\lambda$ ,  $hdr$  and  $hds$ ,  $pbr$  and  $pbs$  and  $m$  are the  
61 carrier-phase measurements, in meter, the geometric distance between satellite and  
62 receiver antennas, in meters, the speed of light, in meters per second, the receiver  
63 and satellite clock errors, respectively, in seconds, the neutral troposphere delay, in  
64 meters, the ionosphere delay, in meters, the carrier-phase integer ambiguity, the  
65 carrier-phase wave length, in meters, the receiver and satellite carrier-phase  
66 hardware delays, respectively, in metric units, the receiver and satellite carrier-  
67 phase initial phase bias, respectively, in metric units, the carrier-phase multipath, in  
68 meters, respectively and  $e$  is the un-modeled errors of carrier-phase measurements,  
69 in meters.



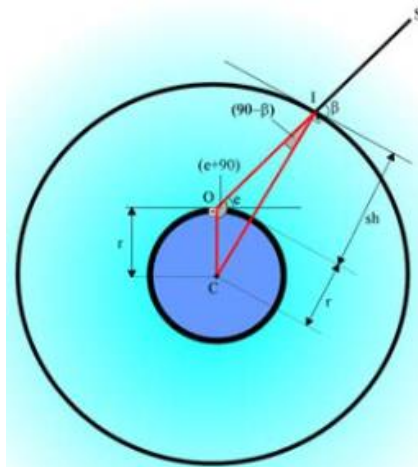
70 **3. Ionospheric Delay Estimation by Geometry-Free Linear Combination of**  
 71 **GPS Observables.**

72 The geometry-free linear combination of GPS observations is classically used for  
 73 ionospheric investigations. It can be obtained by subtracting simultaneous pseudo  
 74 range (P1-P2 or C1-P2) or carrier phase observations ( $\Phi_1-\Phi_2$ ). With this  
 75 combination, the satellite – receiver geometrical range and all frequency  
 76 independent biases are removed (Ciraolo et al., 2007). The ionospheric estimation is  
 77 performed using the following model (Leandro,2009):

78 
$$\phi_{GF} = \phi_{L1} - \phi_{L2} = (1 - \gamma)MF \left( I_{v,0} + \nabla_{\phi}(\phi_p - \phi_0) + \nabla_{\lambda}(\lambda_p - \lambda_0) \right) + Nb'_{gf} \quad (2)$$

79 where  $\phi_{GF}$  is the geometry-free carrier-phase observation in length units, MF is the  
 80 ionosphere mapping function,  $I_{v,0}$  is the vertical ionospheric delay at the station  
 81 position,  $\nabla \phi$  and  $\nabla \lambda$  are latitudinal and longitudinal gradients, respectively,  $\phi_p$   
 82 and  $\lambda_p$  are the geodetic latitude and longitude of the ionospheric piercing point,  $\phi_0$   
 83 and  $\lambda_0$  are the geodetic latitude and longitude of the station,  $\gamma$  is the factor to convert  
 84 the ionospheric delay from L1 to L2 frequency, unitless and  $Nb'_{gf}$  is an ambiguity  
 85 parameter which includes the carrier-phase integer ambiguity plus a collection of  
 86 biases. The mapping function is based on a spherical ionospheric shell model as  
 87 shown in Figure 1, and is computed according to (Leandro,2009):

88 
$$MF = \sqrt{1 - \left( \frac{r}{(r+sh)} \cos(e) \right)^2} \quad (3)$$



89 **Figure (1):** Elements of the ionospheric shell model (Leandro,2009).



90 where  $r$  is the mean radius of earth,  $sh$  is the ionospheric shell height (default value  
 91 is 350 km),  $\beta$  is the satellite elevation angle at the shell height piercing point, and  $e$   
 92 is the elevation angle of satellite S from station O as seen in Figure (1).

93 To compute elevation and azimuth angle for any satellite ( $e$ ,  $Azim$ ), the receiver  
 94 position in Earth Centered Earth Fixed (ECEF) is converted to geodetic coordinate  
 95 ( $\lambda, \varphi, z$ ). Then, the satellite position coordinate ( $x_s, y_s, z_s$ ) from ECEF at the specified  
 96 epoch is interpolated from the IGS final orbits. The interpolated satellite position is  
 97 then transformed to a local coordinate frame, East, North, and Up (ENU) system.  
 98 The transferred ENU is used to calculate elevation and azimuth angles as follows  
 99 (Dahiraj, 2013 and Sedeek et al, 2017):

$$100 \quad e = \tan^{-1} \left( \frac{X_U}{\sqrt{X_N^2 + X_E^2}} \right) \quad (4)$$

$$101 \quad Azim = \tan^{-1} \left( \frac{X_E}{X_N} \right) \quad (5)$$

102 Where  $e$ ,  $Azim$  are the elevation and azimuth angle of satellite at the receiver station  
 103 respectively and  $X_E$ ,  $X_N$ ,  $X_U$  are the satellite position in local coordinate frame.

104 Usually, the ionosphere is assumed to be concentrated on a spherical shell located  
 105 at altitude (nominally taken as 350 km above Earth's surface. Ionospheric Pierce  
 106 Point is the intersection point between the satellite receiver line-of-sight, and the  
 107 ionosphere shell as shown in Figure (1).

108 IPP location can be computed by providing reference station coordinate ( $\phi_0, \lambda_0$ ),  
 109 then the geographic latitude and longitude of IPP can be computed according to  
 110 elevation and azimuth angle of satellite (Dahiraj, 2013). The offset angle between  
 111 the IPP and the receiver ( $\psi$ ) is defined as the offset between the IPP and the user's  
 112 receiver. The elevation angle  $\beta$  and the offset angle between the IPP and the receiver  
 113  $\psi$  are computed as follow (El-Gizawy, 2003):

$$114 \quad \beta = \cos^{-1} \left( \left( \frac{r}{r+sh} \right) \cos(e) \right) \quad (6)$$

$$115 \quad \psi = \beta - e = \cos^{-1} \left( \left( \frac{r}{r+sh} \right) \cos(e) \right) - e \quad (7)$$

116 Where  $r$  and  $sh$  are the mean radius of the spherical Earth and the height of IPP,  
 117 respectively. Given the user's receiver coordinates ( $\phi_0, \lambda_0$ ), and the offset angle  $\psi$ ,  
 118 the pierce point coordinates ( $\phi_{IPP}, \lambda_{IPP}$ ) are then derived by the following  
 119 expressions (El-Gizawy, 2003):



120  $\phi_{IPP} = (\phi_r + \Psi \cos(\text{Azim}))$  (8)

121  $\lambda_{IPP} = \left( \lambda_r + \frac{\Psi \sin(\text{Azim})}{\cos(\phi_{IPP})} \right)$  (9)

122 The ionospheric estimation is performed by means of sequential least-squares  
 123 adjustment, where the parameters are the ionospheric model elements (vertical delay  
 124 and gradients) and the ambiguities as follows:

125  $L=AX$  (10)

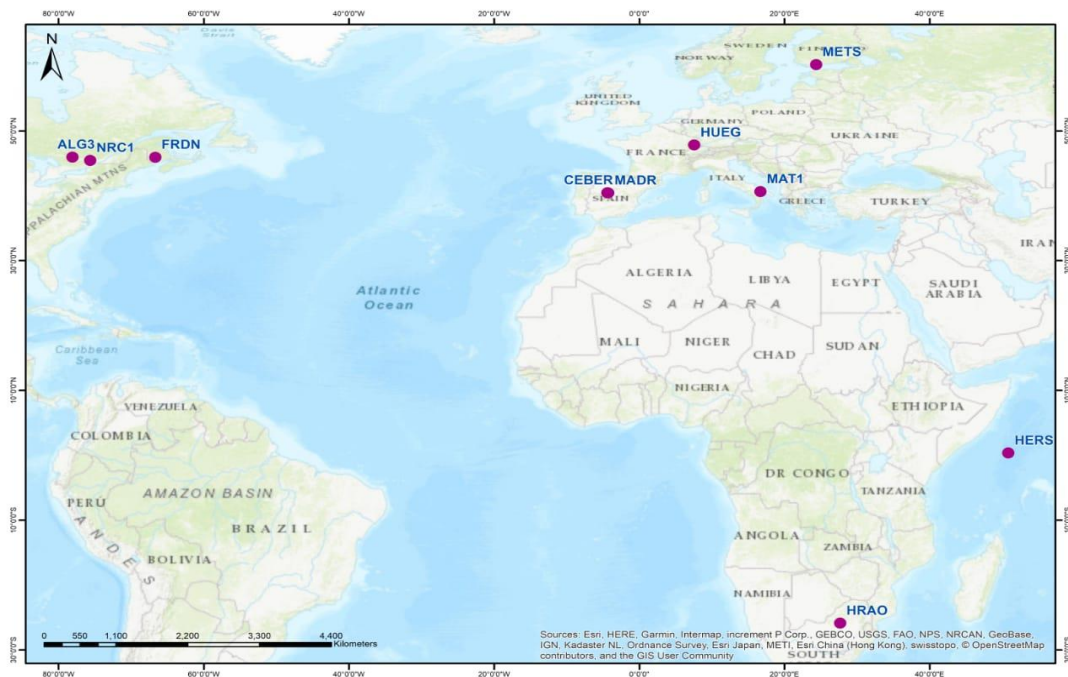
126 Where:  $L$  is the vector of observations,  $A$  is the design matrix,  $X$  is unknown  
 127 parameters vector, and  $P$  is weight matrix of observations.

128  $X = (A_1^T \cdot P_1 \cdot A_1 + A_2^T \cdot P_2 \cdot A_2)^{-1} (A_1^T \cdot P_1 \cdot L_1 + A_2^T \cdot P_2 \cdot L_2)$  (11)

129 By using this system of equations, vertical ionospheric delay, latitudinal and  
 130 longitudinal gradients values at the station position are computed on an epoch by  
 131 epoch basis.

132 **4. Results and Discussions**

133 In the present contribution, to evaluate the performance of the proposed model,  
 134 numerical case-studies were performed on ten IGS stations. These stations are  
 135 shown in Figure (2).

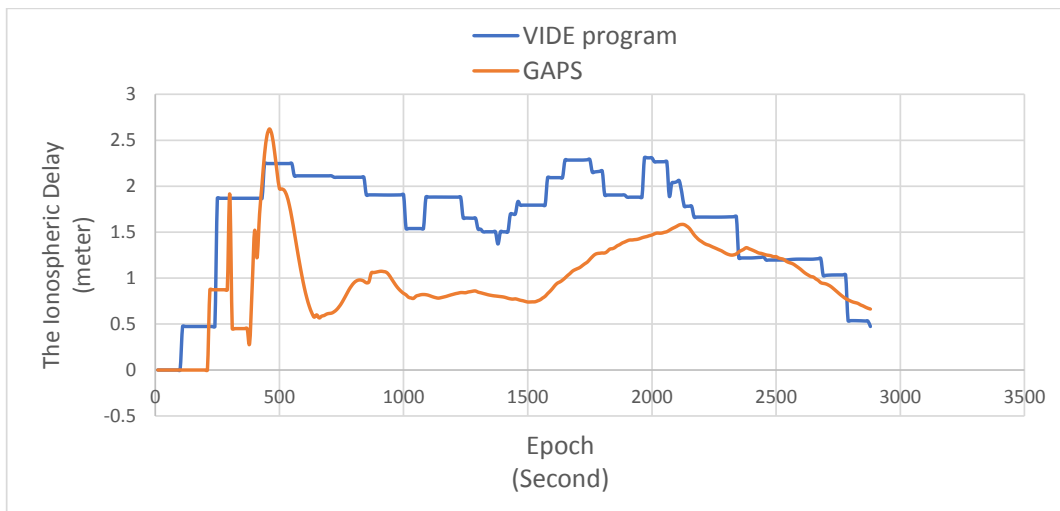


136  
 137

Figure (2): IGS stations which were used in this study.

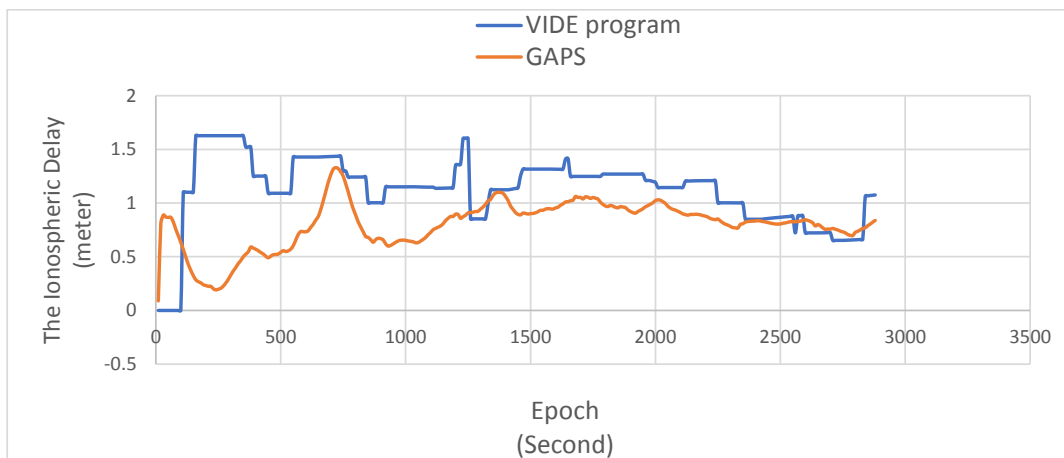


138 The Ionosphere delay is estimated for observations of Doy 3, 2018 for these  
139 stations and the results were compared with the results of the online version of the  
140 GPS Analysis and Positioning Software (GAPS) as shown in the following  
141 figures:



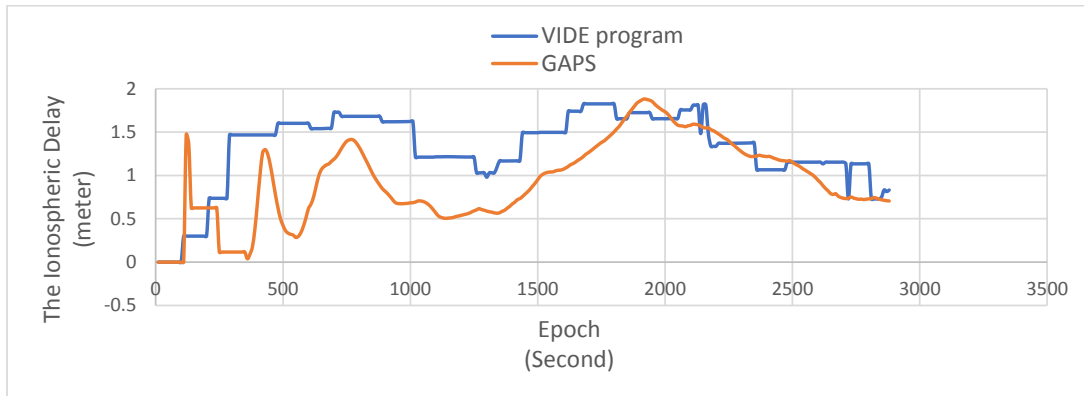
142

143 **Figure (3):** Vertical Ionosphere delay of ALGO station estimated by the VIDE program and GAPS of DOY 3, 2018.



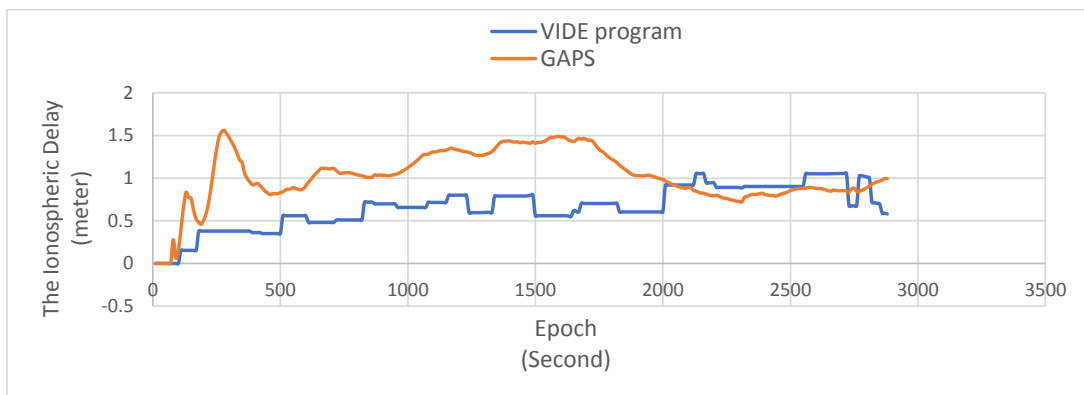
144

145 **Figure (4):** Vertical Ionosphere delay of CEBR station estimated by the VIDE program and GAPS of DOY 3, 2018.



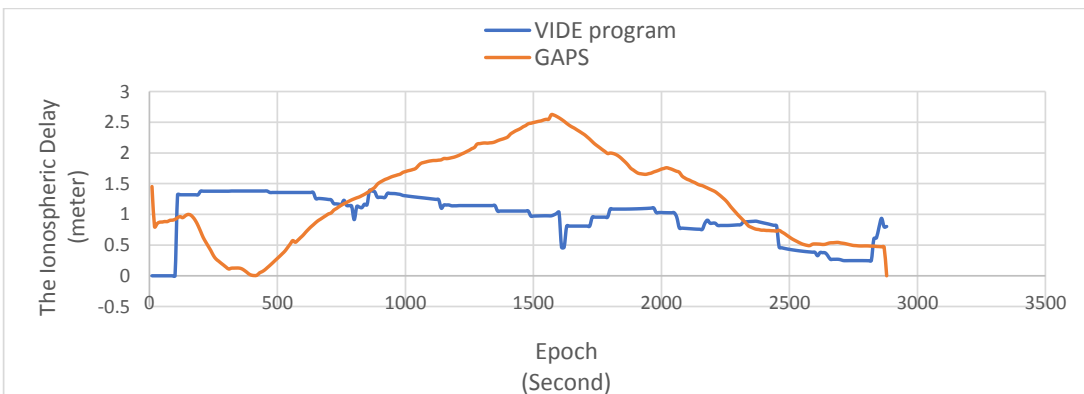
146

147 **Figure (5):** Vertical Ionosphere delay of FRDN station estimated by the VIDE program and GAPS of DOY 3, 2018.



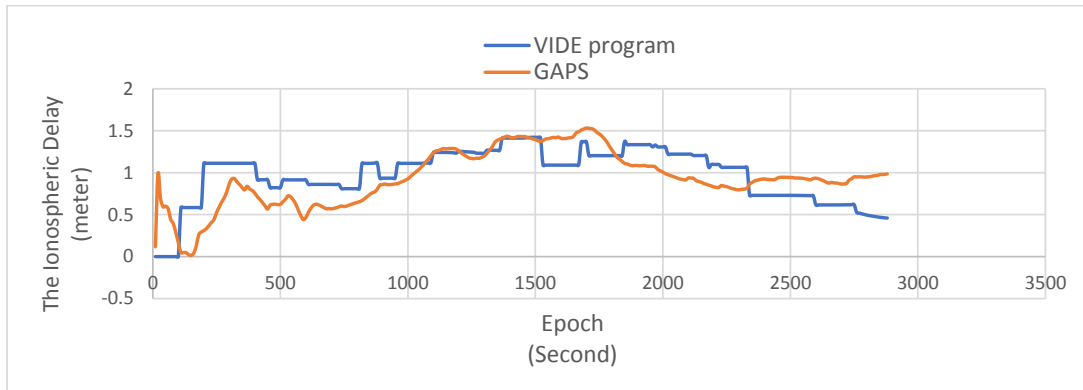
148

149 **Figure (6):** Vertical Ionosphere delay of HERS station estimated by the VIDE program and GAPS of DOY 3, 2018.



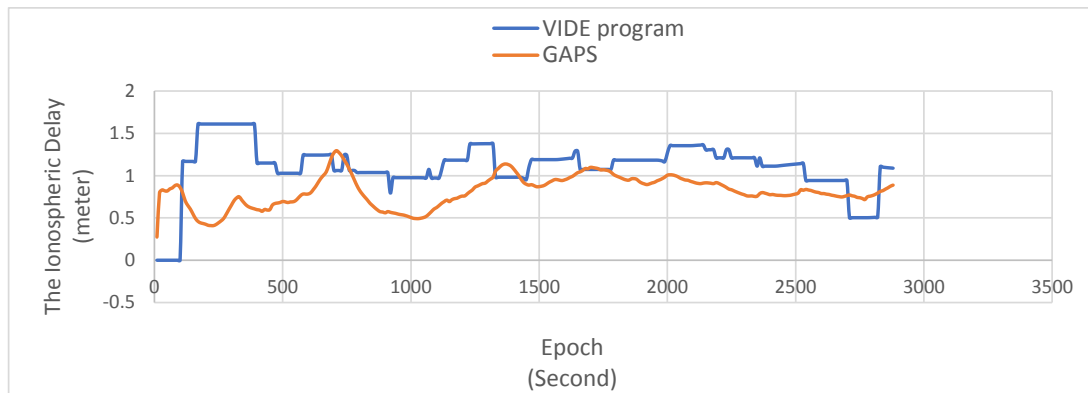
150

151 **Figure (7):** Vertical Ionosphere delay of HRAO station estimated by VIDE program and GAPS of DOY 3, 2018.



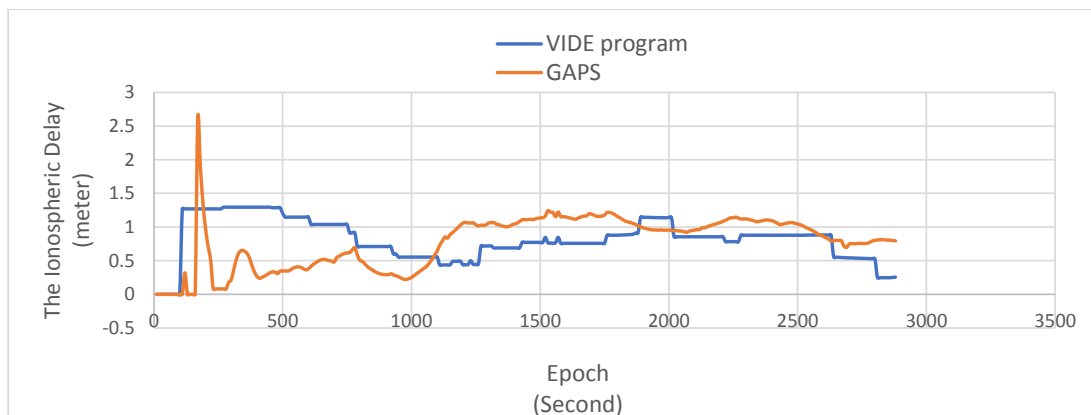
152

153 **Figure (8):** Vertical Ionosphere delay of HUEG station estimated by the VIDE program and GAPS of DOY 3, 2018.



154

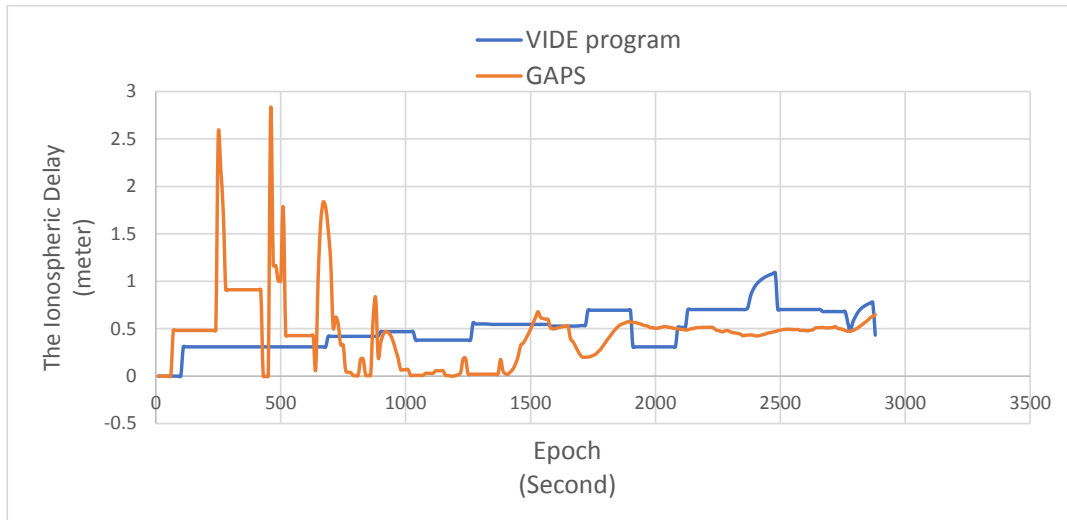
155 **Figure (9):** Vertical Ionosphere delay of MADR station estimated by VIDE program and GAPS of DOY 3, 2018.



156

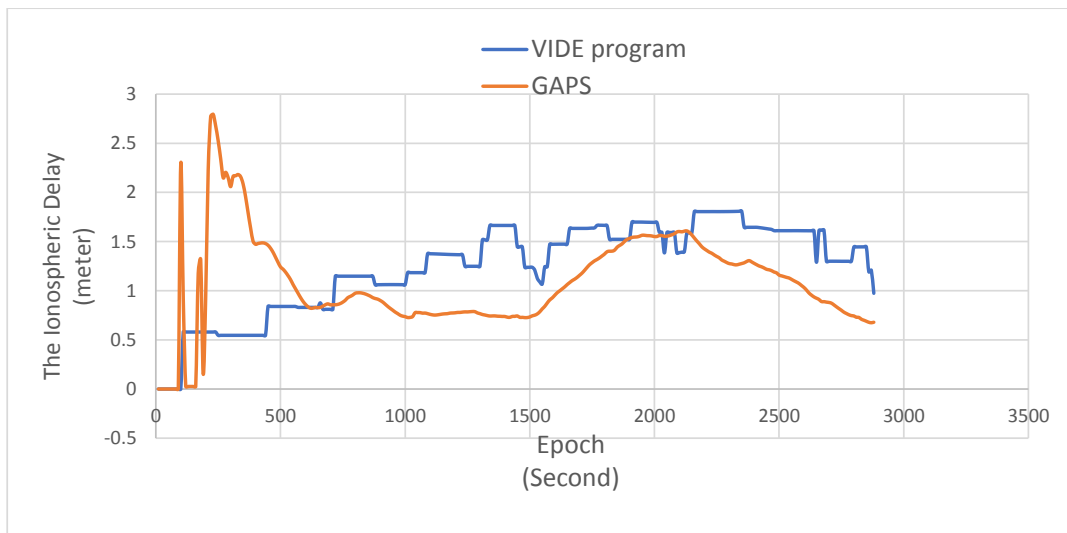
157 **Figure (10):** Vertical Ionosphere delay of MAT1 station estimated by VIDE program and GAPS of DOY 3, 2018.





158

159 **Figure (11):** Vertical Ionosphere delay of METS station estimated by VIDE program and GAPS of DOY 3, 2018.



160

161 **Figure (12):** Vertical Ionosphere delay of NRC1 station estimated by VIDE program and GAPS of DOY 3, 2018.

162 Previous figures show a comparison of the ionospheric delays computed with the  
163 proposed code and GAPS. This comparison shows how much the accuracy of this  
164 study is good in terms of agreement of solutions provided by GAPS.



165 **Table (1):** The average Ionospheric Delay of each station of DOY 3, 2018 using the  
 166 Proposed code and GAPS.

Average Ionospheric Delay (m)			Average Ionospheric Delay (m)		
Station	Proposed Code	GAPS	Station	Proposed Code	GAPS
<b>ALGO</b>	1.6205	0.9996	<b>HUEG</b>	0.9790	0.9328
<b>CEBER</b>	1.1203	0.7948	<b>MADR</b>	1.6838	0.8126
<b>FRDN</b>	1.3139	0.9387	<b>MAT1</b>	0.8189	0.9771
<b>HERS</b>	0.6594	1.0255	<b>METS</b>	0.4961	0.5106
<b>HRAO</b>	0.9681	1.2758	<b>NRC1</b>	1.2463	1.0848

167 **5.CONCLUSIONS**

168 We have overviewed an algorithm which can be used to estimate ionospheric delays  
 169 of GPS observations using single GPS receiver using a spherical ionospheric shell  
 170 model. This Algorithm depends on the geometry-free carrier-phase observations  
 171 after detecting cycle slip. The ionospheric estimation in this algorithm is performed  
 172 by means of Sequential least-squares adjustment. This study is performed on ten IGS  
 173 stations. Previous figures and table (1) show an agreement of the proposed code  
 174 results and values provided by GAPS. This procedure may be better than GAPS  
 175 because it can estimate the ionospheric delays each thirty seconds whereas GAPS  
 176 estimate the ionospheric delays each ten minutes.

177  
 178 **6. References:**

- 179 *Ciraolo, L., Azpilicueta, F., Brunini, C., Meza, A., and Radicella S., M.:* Calibration errors on  
 180 experimental Slant Total Electron Content (TEC) determined with GPS, Journal of Geodesy,  
 181 Vol. 81, No. 2, pp. 111–120, 2007.
- 182 *Deng, Z., M., Bender G. Dick, Ge M., Wickert J., Ramatschi M., and Zou X.:* Retrieving  
 183 tropospheric delays from GPS networks densified with single frequency receivers.  
 184 Geophysical Research Letters, VOL. 36, L19802, doi:10.1029/2009GL040018, 2009.
- 185 *Dahira jsunehra.:* Validation of GPS receiver instrumental bias results for precise navigation.  
 186 Indian Journal of Radio& space Physics, Vol. 42June 2013. pp.175-181, 2013.



- 187 **El-Gizawy, M. L.:** Development of An Ionosphere Monitoring Technique Using GPS  
188 Measurements for High Latitude GPS Users. Master of Science. University of Calgary,  
189 Canada, 2003.
- 190 **Guochang Xu.:** GPS Theory, Algorithms and Applications, Library of Congress Control Number:  
191 2007929855. ISBN second edition 978-3-540-72714-9 Springer Berlin Heidelberg New York,  
192 2007.
- 193 **Hofmann-Wellenhof, B., Lichtenegger H., and WalseE.:** GNSS Global Navigation Satellite  
194 Systems; GPS, Glonass, Galileo & more, Springer Wien, New York, 2008.
- 195 **Jakobsen J., Knudsen P., Jensen A.:** Analysis of local ionospheric time varying characteristics  
196 with singular value decomposition, Journal of Geodesy 85 (7) pages 449-456,  
197 <http://dx.doi.org/10.1007/s00190-010-0378-2>. Special Issue on the 43rd ISCIIE International  
198 Symposium on Stochastic, 2010.
- 199 **Komjathy, A.:** Global Ionospheric Total Electron Content Mapping Using the Global Positioning  
200 System, Ph.D. dissertation, Department of Geodesy and Geomatics Engineering Technical  
201 Report No. 188, University of New Brunswick, Fredericton, New Brunswick, Canada, 248 p,  
202 1997.
- 203 **Leandro R. F.:** Precise Point Positioning with GPS: A New Approach for Positioning,  
204 Atmospheric Studies, and Signal Analysis, Ph.D. dissertation, Department of Geodesy and  
205 Geomatics Engineering, Technical Report No. 267, University of New Brunswick,  
206 Fredericton, New Brunswick, Canada, 232 pp, 2009.
- 207 **Masaharu Ohashi, Taisuke Hattori, Yukihiko Kubo and Suetoshi Sugimoto.:** Multi-Layer  
208 Ionospheric VTEC Estimation for GNSS Positioning, special Issue on the 43rd ISCIIE  
209 International Symposium on Stochastic Systems Theory and Its Applications-III Vol. 26, No.  
210 1, pp. 16–24, 2013.
- 211 **Sedeek A. A., Doma M. I., Rabah M. and Hamama M. A.:** Determination of Zero Difference  
212 GPS Differential Code Biases for Satellites and Prominent Receiver Types, Arabian journal of  
213 geosciences, vol. 10, January 2017.
- 214 **Schaer, S.:** Mapping and Predicting the Earth's Ionosphere Using the Global Positioning System,  
215 PhD dissertation, Astronomical Institute, University of Berne, Switzerland, pp. 205, 1997.
- 216 **Wielgosz P., L.W. Baran, I.I. Shagimuratov and M.V. Aleshnikova (2003a).:** Latitudinal  
217 variations of TEC over Europe obtained from GPS observation, accepted by Annales  
218 Geophysicae, 2003.
- 219 **Wielgosz, P., Grejner-Brzezinka, D. and Kashani, I. (2003b).:** Regional Ionosphere Mapping  
220 with Kriking and Multiquadric Methods, Journal of Global Positioning Systems, vol. 2, no. 1,  
221 pp 48-55, 2003.